INTERNATIONAL JOURNAL FOR NUMERICAL METHODS IN FLUIDS
*Int. J. Numer. Meth. Fluids* 2007; **53**:811–826
Published online 2 August 2006 in Wiley InterScience (www.interscience.wiley.com). DOI: 10.1002/fld.1305

# Simulation of rapidly varying flow using an efficient TVD–MacCormack scheme

Dongfang Liang[‡], Binliang Lin[§] and Roger A. Falconer[*,†]

*Hydroenvironmental Research Centre, Cardiff School of Engineering, Cardiff University, The Parade, Cardiff CF24 3AA, U.K.*

SUMMARY

An efficient numerical scheme is outlined for solving the SWEs (shallow water equations) in environmental flow; this scheme includes the addition of a five-point symmetric total variation diminishing (TVD) term to the corrector step of the standard MacCormack scheme. The paper shows that the discretization of the conservative and non-conservative forms of the SWEs leads to the same finite difference scheme when the source term is discretized in a certain way. The non-conservative form is used in the solution outlined herein, since this formulation is simpler and more efficient. The time step is determined adaptively, based on the maximum instantaneous Courant number across the domain. The bed friction is included either explicitly or implicitly in the computational algorithm according to the local water depth. The wetting and drying process is simulated in a manner which complements the use of operator-splitting and two-stage numerical schemes. The numerical model was then applied to a hypothetical dam-break scenario, an experimental dam-break case and an extreme flooding event over the Toce River valley physical model. The predicted results are free of spurious oscillations for both sub- and super-critical flows, and the predictions compare favourably with the experimental measurements. Copyright © 2006 John Wiley & Sons, Ltd.

Received 20 January 2006; Revised 20 April 2006; Accepted 10 June 2006

KEY WORDS: shallow water flows; dam-break; numerical modelling; total variation diminishing; shock capturing; conservation laws

*Correspondence to: Roger A. Falconer, Hydroenvironmental Research Center, Cardiff School of Engineering, Cardiff University, The Parade, Cardiff CF24 3AA, U.K.
†E-mail: FalconerRA@cf.ac.uk
‡E-mail: liangd@cf.ac.uk
§E-mail: linbl@cf.ac.uk

Contract/grant sponsor: Engineering and Physical Sciences Research Council; contract/grant number: GR/S76304

## INTRODUCTION

The SWEs have been widely used in predicting large-scale coastal and inland flow processes, particularly since the advent of computer solutions of these equations from the mid-20th century onwards. Due to the existence of the free surface, the SWEs are mathematically similar to the Euler equations. For example, discontinuities may arise in the solution due to the hyperbolic nature of these equations. These discontinuities are often described as shocks, jumps or bores. They are commonplace when the Froude number approaches, or exceeds, unity. Such types of rapidly varying flows can be found in mountainous rivers, storm surges, the sudden opening of sluice gates, dam-breaks, levee breaches, flash floods, etc.

Traditionally, the SWEs have been frequently solved using the alternating direction implicit (ADI) method, which has been very successful in balancing numerical accuracy with computational efficiency (e.g. References [1–3]). This method works well when the flow is slow and smooth, i.e. when the Froude number is much less than unity. Recently, more effort has been focused on numerically predicting the formation and propagation of shocks in free surface flows, which are beyond the capabilities of the classical ADI-type numerical solution algorithms. The shock imposes a great challenge to numerical schemes, as it means a vertical change of flow conditions. Theoretically, no matter how fine is the grid, the sharp change always occurs within one grid interval.

Shock-fitting and shock-capturing are two approaches for resolving discontinuities in the solution of general hyperbolic equations. The shock-fitting approach isolates the shock from adjacent smooth regions and treats it separately as a moving internal boundary (e.g. References [4, 5]). However, it may be hard to detect and track the shocks accurately if there are many of them appearing and disappearing with time in an unsteady flow problem. Due to this difficulty, the shock-capturing methods have become preferable to the shock-fitting methods [6, 7]. The shock-capturing methods utilize a universal solution strategy over the whole domain, regardless of the discontinuities or smooth regions. Therefore, there is no limit on the number and direction of shocks.

Although the SWEs describe the mass and momentum conservation of the flows, not all of the numerical schemes for the SWEs can inherit the conservative property. The shock-capturing method requires the numerical schemes to preserve the conservation law in a discrete fashion. There have been two major families of shock-capturing schemes in use in computational fluid dynamics. One is the Godunov method, which solves Riemann problems at the interfaces of grid cells (e.g. References [7–9]). The other is the arithmetical combination method of 1st- and 2nd-order upwind schemes (e.g. References [10–13]). The TVD–MacCormack method outlined in this paper belongs to the second category.

Although a number of shock-capturing methods have been proposed, they are generally time-consuming and have been applied mainly to relatively simple flow conditions. The purpose of this paper is to develop an efficient solver that can be used for complex flows in practical situations. The MacCormack explicit predictor–corrector scheme has been chosen as the basic numerical scheme. A simple TVD step has been added so that the oscillations are eliminated in high-gradient regions while at the same time second-order accuracy is still retained. Usually the conservative form of the governing equations is used in deriving shock-capturing schemes to ensure that the discrete solution satisfies mass and momentum conservation. It is shown in this paper that by discretizing the non-conservative form of the SWEs in a certain manner, the finite difference scheme also has the conservative property. Furthermore, the computational cost can be reduced by employing the non-conservative form of the SWEs. The efficiency has been further enhanced by using an adaptive



DOI: 10.1002/fld

time step in the computations. The present TVD–MacCormack model was firstly verified against hypothetical and experimental dam-break problems in this paper. Then it was used to simulate an extreme flood event in a natural environment, where bed friction, wetting and drying, embankment overtopping, and flow transitions were all included. The predicted results agreed well with the laboratory measurements.

## GOVERNING EQUATIONS

Disregarding the Coriolis, wind and viscous forces, the general form of the SWEs can be written as

$$\frac{\partial \eta}{\partial t} + \frac{\partial q_x}{\partial x} + \frac{\partial q_y}{\partial y} = 0 \tag{1}$$

$$\frac{\partial q_x}{\partial t} + \frac{\partial \left(\frac{\beta q_x^2}{H}\right)}{\partial x} + \frac{\partial \left(\frac{\beta q_x q_y}{H}\right)}{\partial y} = -gH\frac{\partial \eta}{\partial x} - \frac{g q_x \sqrt{q_x^2 + q_y^2}}{H^2 C^2} \tag{2}$$

$$\frac{\partial q_y}{\partial t} + \frac{\partial \left(\frac{\beta q_x q_y}{H}\right)}{\partial x} + \frac{\partial \left(\frac{\beta q_y^2}{H}\right)}{\partial y} = -gH\frac{\partial \eta}{\partial y} - \frac{g q_y \sqrt{q_x^2 + q_y^2}}{H^2 C^2} \tag{3}$$

where $t$ is time; $\eta$ is the water surface elevation above datum; $q_x$ and $q_y$ are the discharge per unit width components in the $x$ and $y$ directions, respectively; $\beta$ is the correction factor for the non-uniform vertical velocity profile, which equates to 1.0 for a uniform velocity distribution and 1.016 for a seventh power law velocity distribution; $H(=h+\eta)$ is the total water column depth, with $h$ being the water depth below datum; $g$ is the acceleration due to gravity; and $C$ is the Chezy roughness value.

These are usually called the non-conservative formulation of the SWEs, because the source term does not equate to zero when neglecting the bed topography variance and bottom friction. The water surface gradient term on the right-hand side of Equations (2) and (3) can be re-written as (e.g. References [9, 14])

$$-gH\frac{\partial \eta}{\partial x} = -\frac{\partial \left(\frac{g\eta^2}{2} + gh\eta\right)}{\partial x} + g\eta\frac{\partial h}{\partial x} \tag{4}$$

$$-gH\frac{\partial \eta}{\partial y} = -\frac{\partial \left(\frac{g\eta^2}{2} + gh\eta\right)}{\partial y} + g\eta\frac{\partial h}{\partial y} \tag{5}$$



DOI: 10.1002/fld

with the momentum Equations (2) and (3) correspondingly being changed to give

$$\frac{\partial q_x}{\partial t} + \frac{\partial\left(\dfrac{\beta q_x^2}{H} + \dfrac{g\eta^2}{2} + gh\eta\right)}{\partial x} + \frac{\partial\left(\dfrac{\beta q_x q_y}{H}\right)}{\partial y} = g\eta\frac{\partial h}{\partial x} - \frac{gq_x\sqrt{q_x^2+q_y^2}}{H^2C^2} \tag{6}$$

$$\frac{\partial q_y}{\partial t} + \frac{\partial\left(\dfrac{\beta q_x q_y}{H}\right)}{\partial x} + \frac{\partial\left(\dfrac{\beta q_y^2}{H} + \dfrac{g\eta^2}{2} + gh\eta\right)}{\partial y} = g\eta\frac{\partial h}{\partial y} - \frac{gq_y\sqrt{q_x^2+q_y^2}}{H^2C^2} \tag{7}$$

The formulation given in Equations (1), (6), (7) is called the conservative form of the SWEs, as the source terms will be zero on frictionless flat beds. The non-conservative and conservative formulations of the SWEs are equivalent to each other mathematically. In order to insure the correct conservations of mass and momentum in the discrete form, the governing equations are usually transformed into their conservative form before being solved numerically. However, it should be borne in mind that what really matters is the conservative property of the final difference equations, rather than the mere usage of the conservative type of differential equations.

## SOLUTION METHODS

### *TVD–MacCormack scheme*

The solution of the 2-D SWEs can be decomposed into the solution of two sets of 1-D equations in each time step based on the operator-splitting technique, the details of which can be found in References [10, 15]. Therefore, only the variance in the $x$ direction is considered in this section. To facilitate the subsequent description of the numerical scheme, the generalized 1-D equation is introduced accordingly

$$\frac{\partial U}{\partial t} + \frac{\partial F}{\partial x} = S \tag{8}$$

where $U$ represents $\eta$, $q_x$ or $q_y$; and $F$ and $S$ represent the flux and source terms, respectively, in the corresponding equation.

An explicit TVD–MacCormack finite difference scheme has been employed to solve Equation (8). A five point, symmetric TVD term [16–18] has been added to the corrector step, so as to remove the numerical oscillations near sharp gradients. The overall scheme includes two steps in each time marching, giving

$$\overline{U_i^{n+1}} = U_i^n - (F_i^n - F_{i-1}^n)\cdot\Delta t/\Delta x + S^n\cdot\Delta t \tag{9}$$

$$U_i^{n+1} = 0.5\cdot\left[\overline{U_i^{n+1}} + U_i^n - (\overline{F_{i+1}^{n+1}} - \overline{F_i^{n+1}})\cdot\Delta t/\Delta x + \overline{S^{n+1}}\cdot\Delta t\right] + TVD_i \tag{10}$$

where the superscript and subscript refer to the temporal and spatial indices, respectively, and

$$TVD_i = [G(r_i^+) + G(r_{i+1}^-)]\cdot\Delta U_{i+1/2}^n - [G(r_{i-1}^+) + G(r_i^-)]\cdot\Delta U_{i-1/2}^n \tag{11}$$



DOI: 10.1002/fld

in which

$$\Delta U^n_{i+1/2} = U^n_{i+1} - U^n_i \tag{12a}$$

$$\Delta U^n_{i-1/2} = U^n_i - U^n_{i-1} \tag{12b}$$

$$r_i^+ = \frac{\Delta\eta^n_{i-1/2}\cdot\Delta\eta^n_{i+1/2} + \Delta q^n_{x_{i-1/2}}\cdot\Delta q^n_{x_{i+1/2}} + \Delta q^n_{y_{i-1/2}}\cdot\Delta q^n_{y_{i+1/2}}}{\Delta\eta^n_{i+1/2}\cdot\Delta\eta^n_{i+1/2} + \Delta q^n_{x_{i+1/2}}\cdot\Delta q^n_{x_{i+1/2}} + \Delta q^n_{y_{i+1/2}}\cdot\Delta q^n_{y_{i+1/2}}} \tag{13a}$$

$$r_i^- = \frac{\Delta\eta^n_{i-1/2}\cdot\Delta\eta^n_{i+1/2} + \Delta q^n_{x_{i-1/2}}\cdot\Delta q^n_{x_{i+1/2}} + \Delta q^n_{y_{i-1/2}}\cdot\Delta q^n_{y_{i+1/2}}}{\Delta\eta^n_{i-1/2}\cdot\Delta\eta^n_{i-1/2} + \Delta q^n_{x_{i-1/2}}\cdot\Delta q^n_{x_{i-1/2}} + \Delta q^n_{y_{i-1/2}}\cdot\Delta q^n_{y_{i-1/2}}} \tag{13b}$$

The function $G()$ in Equation (11) is defined as

$$G(x) = 0.5 \times C \times [1 - \phi(x)] \tag{14}$$

where the flux limiter function is given as

$$\phi(x) = \max(0, \min(2x, 1)) \tag{15}$$

and the variable $C$ is

$$C = \begin{cases} Cr \times (1 - Cr), & Cr \leqslant 0.5 \\ 0.25, & Cr > 0.5 \end{cases} \tag{16}$$

with $Cr$ being the local Courant number and defined as

$$Cr = \frac{(|q_x/H| + \sqrt{gH})\Delta t}{\Delta x} \tag{17}$$

One benefit of using the predictor–corrector two-stage scheme is that the source term can be treated easily, so that the whole scheme has second-order accuracy in both time and space. Furthermore, since no apparent characteristic transformation is needed in the present TVD–MacCormack scheme, this scheme is efficient in comparison with most other shock-capturing schemes.

## DEPLOYMENT OF NON-CONSERVATIVE FORM OF THE SWEs

It is particularly important for numerical schemes to comply with the conservation law when being used to simulate flows with discontinuities. Because of the nonlinearity of the SWEs, the numerical solutions for the conservative and non-conservative formulations are usually different, even though the local acceleration, advective acceleration and bed friction terms are discretized in the same manner. However, the numerical schemes for the conservative and non-conservative formulations can be derived from each other if the relationships described in Equations (4) and (5) still hold in finite difference schemes. Only Equation (4) in the predictor step, where the spatial derivative is approximated by a backward difference, is examined in the following analysis. A similar analysis can be carried out for the corrector step and for Equation (5). Omitting the temporal indices in the superscript, the right hand side of Equation (4) can be discretized as follows:

$$-\frac{g\eta_i^2 - g\eta_{i-1}^2}{2\Delta x} - \frac{gh_i\eta_i - gh_{i-1}\eta_{i-1}}{\Delta x} + g\,\frac{\eta_{i-1} + \eta_i}{2}\,\frac{h_i - h_{i-1}}{\Delta x} \tag{18}$$



DOI: 10.1002/fld

With some algebraic manipulation, it is not difficult to transform Equation (18) into a simpler form:

$$-g\,\frac{H_{i-1}+H_i}{2}\,\frac{\eta_i-\eta_{i-1}}{\Delta x} \tag{19}$$

Equation (19) can be deemed as the finite difference discretization for left-hand side of Equation (4). In other words, the finite difference schemes for Equations (2) and (6) will be exactly the same if the term $-gH\,\partial\eta/\partial x$ in Equation (2) is approximated by Equation (19) and the term $g\eta\,\partial h/\partial x$ in Equation (6) is approximated by the third term in Equation (18) in the predictor step. Of course, this argument should be supported by using the same differencing scheme to discretize the other corresponding terms in Equations (2) and (6). Similar conclusions can be drawn for the corrector step and for Equations (3) and (7). Because the SWEs in their non-conservative form, i.e. Equations (1)–(3), are simpler and more efficient for use in the computation, they are preferred in the current numerical solution.

In fact, the non-conservative form of momentum equations defined by Equations (2) and (3) is more straightforward physically, i.e. the water surface gradients ($\partial\eta/\partial x$, $\partial\eta/\partial y$) appear in the source terms explicitly that drive the flow. In the deployment of Equations (6) and (7), care should be taken to discretize the bed slope terms (i.e. $g\eta\,\partial h/\partial x$, $g\eta\,\partial h/\partial y$) on the right-hand side and the flux-gradient terms on the left-hand side of the equations consistently. Otherwise, a numerical imbalance may occur near sharp bed-slope changes, i.e. the water cannot remain still, even though quiescent conditions are applied (e.g. References [9, 19, 20]). Some bench mark test cases, which involve the TVD–MacCormack scheme, can also be found in Reference [15]. Equation (18) indicates that a balance can be achieved by approximating the water levels in bed slope terms in Equations (6) and (7) with the arithmetic average in the direction of difference.

*Adaptive time step algorithm*

As for all explicit methods, the maximum time step is subject to the stability restriction given by the well-known Courant–Friedrich–Lewy (CFL) condition. In order to accelerate the computation, the time step is adjusted dynamically according to a fixed maximum Courant number, given as

$$\Delta t = Cr_{\text{Preset}} \times \frac{\Delta x}{\max\left(\sqrt{q_x^2+q_y^2}/H+\sqrt{gH}\right)} \tag{20}$$

where $Cr_{\text{Preset}}$ is a preset quantity and max( ) denotes the maximum value across the entire computational domain. It is expected that the time step will automatically be small when the flow changes rapidly and *vice versa*. To enhance the accuracy and stability of the model, the time step variance is confined in a predetermined range.

*Wetting/drying algorithm*

In some research studies, the complex wetting/drying phenomenon is simulated by imposing a thin layer of water across dry cells (e.g. References [12, 13]). In this way, the computation is always carried out everywhere regardless of the wet/dry condition. However, this simple treatment is not suitable for uneven ground situations, where the dry area must be recognized and excluded from the normal finite difference computation. Otherwise, water level gradients over relatively steep dry grounds will induce unreasonably large velocities.



DOI: 10.1002/fld

At the beginning of each step, all the grid points whose depths are smaller than a prescribed value, $H_{\min}$, are regarded as being dry. The water depth is frozen and the velocities are set to zero at dry grid points. This drying examination is followed by a wetting examination, where the neighbouring grid points around each dry grid point are examined. Nothing is done to the central dry grid point, if all its neighbouring grid points are dry or all of its neighbouring wet grid points have lower water levels than the ground level of the central dry grid point. If the highest water level on the neighbouring wet grid points is $2H_{\min}$ higher than the ground level at the central dry grid point, then the water level on the central dry grid point will be increased by $H_{\min}$. And correspondingly, the water level at the nearby wet grid point will be decreased by $H_{\min}$ to maintain the overall mass balance. Then, another drying examination is performed, thus the newly-wetted grid points will be included in the following computation. The subsequent finite difference solution is only carried out on the wet grid points. Care has been taken to enforce a no flow condition at the wet/dry interface, so the mass balance in the flow is guaranteed. Under the operator-splitting framework, the special treatment for the wet grid point at the wet/dry interface also consists of the treatments in the $x$ and $y$ directions, respectively, within each time step. Without loss of generality, the two neighbouring wet and dry grid points are assumed to align in the $x$ direction in the following. For the wet grid point at the interface, the $x$-direction velocity component is forced to zero when conducting the standard MacCormack computation, while the water level and $y$-direction velocity are computed normally. The TVD flux between the wet and dry grid points is also assigned to be zero. Detailed numerical experiments have shown that the mass conservation is strictly satisfied in the flow during the wetting/drying processes.

Apart from the CFL constriction, the time step should be small enough to insure that the wetting/drying switchover be limited to within one grid size in each time step. Otherwise, the speed of the wetting/drying front may be incorrectly predicted using the current scheme.

*Bed friction term*

For Equations (2) and (3), the presence of the water depth in the denominator of several terms disallows zero depths. In fact, zero depths are effectively prevented from being involved in the computation by the above-mentioned wetting/drying algorithm. However, a singularity can still arise with regard to the bed friction term when the water depth becomes very small. For small water depths, the bed friction term dominates over other terms in the momentum equation, as the term $H^2C^2$ appears in the denominator. In such a situation the momentum equation can be approximated by retaining only the local acceleration and the bed friction terms, giving in the $x$ direction for instance

$$\frac{\partial q_x}{\partial t} = -\frac{g q_x \sqrt{q_x^2 + q_y^2}}{H^2 C^2} \tag{21}$$

Using an explicit numerical scheme for Equation (21) will severely limit the magnitude of the minimum depth permissible across the domain and the maximum admissible time step for stability constraints [21]. One way of dealing with this is to use a partially implicit approach as follows:

$$\frac{q_x^{n+1} - q_x^n}{\Delta t} = -\left(\frac{g\sqrt{q_x^2 + q_y^2}}{H^2 C^2}\right)^n \cdot q_x^{n+1} \tag{22}$$



DOI: 10.1002/fld

which can be re-formulated as

$$q_x^{n+1} = \frac{q_x^n}{1 + \Delta t \cdot \left( \dfrac{g\sqrt{q_x^2 + q_y^2}}{H^2 C^2} \right)^n} \tag{23}$$

In the present model, an explicit scheme has generally been used for all terms, as normally required by the operator-splitting method. A threshold water depth, $H_{\text{Preset}}$, is given by the user, below which the implicit scheme has been used for discretizing the bed friction term to enhance the robustness of the model.

## APPLICATIONS

### *Hypothetical dam-break problem*

The 2-D asymmetrical dam-break problem has been a benchmark test case for shock-capturing numerical models (e.g. References [7, 10, 11, 14, 17, 22]). A square domain is considered, with a side length of 200 m. The bed is flat and frictionless. A 15 m thick dam at $x = 100$ m initially separates the headwater, with a depth of 10 m, from the tailwater with the depth being denoted by $H_0$. In the current study $H_0$ can be either 5, 0.1 or $10^{-3}$ m. Wall conditions are specified at the outer boundaries normal to the dam, while first-order derivatives of all unknowns are fixed to zero at the outer boundaries parallel to the dam. A breach located at $y = 95$ m–170 m occurs suddenly in the dam. The water surface 7.2 s after the breach is examined in the following analysis, using a time step of 0.2 s and a grid size of 5 m. The adaptive time step function has not been turned on in this example.

The water surface elevations computed by the present TVD–MacCormack scheme are shown in Figure 1, which agree well with those calculated by other researchers. It is noted that the flood wave travels faster with a decrease in the downstream water depth. For example, the wave front has moved outside of the computational domain for the case with $H_0 = 10^{-3}$ m, while the wave has not reached the downstream boundary for the other two situations. On the other hand, the wave front is observed to be steeper when the downstream water depth is larger.

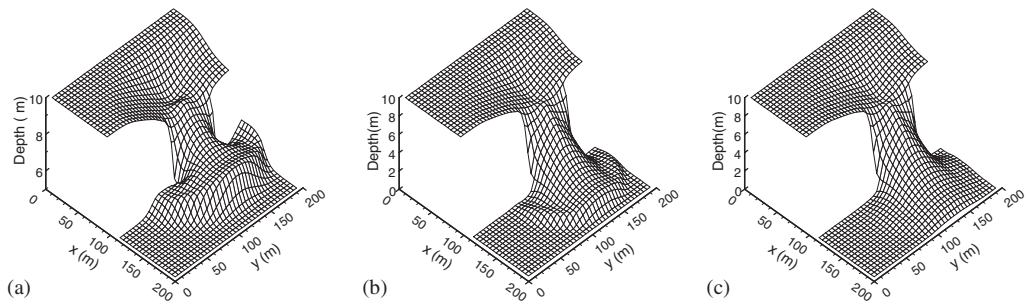


Figure 1. Simulation by TVD–MacCormack scheme for an idealised breach: (a) $H_0 = 5$ m, $H_{\min} = 10^{-5}$ m; (b) $H_0 = 0.1$ m, $H_{\min} = 10^{-5}$ m; and (c) $H_0 = 10^{-3}$ m, $H_{\min} = 10^{-5}$ m.



DOI: 10.1002/fld

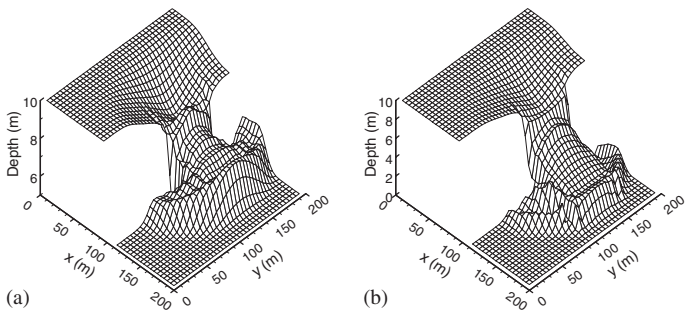


Figure 2. Simulation by standard MacCormack scheme for an idealized breach: (a) $H_0 = 5\,\text{m}$, $H_{\min} = 10^{-5}\,\text{m}$; and (b) $H_0 = 0.1\,\text{m}$, $H_{\min} = 0.1\,\text{m}$.

In order to show the effectiveness of the TVD modifications, the standard MacCormack scheme has also been applied to the same problem. As seen in Figure 2, wild oscillations are generated in the water surface elevations, which are apparently non-physical. Moreover, it was found that $H_{\min}$ had to be increased to 0.1 m for the computations to proceed for $H_0 = 0.1\,\text{m}$ case. For all other runs, $H_{\min}$ was set to $10^{-5}\,\text{m}$. Violent oscillations led to the collapse of the computations at a very early stage when $H_0 = 10^{-3}\,\text{m}$, hence no results are shown for this case. This can be explained by the lower downstream water level posing a more severe test case for numerical models, since part of the flow falls into the super-critical regime.

*Dam-break over a dry floodplain*

A symmetrical dam-break experiment over an initially dry floodplain was performed by Fraccarollo and Toro [23]. The entire domain was $3\,\text{m} \times 2\,\text{m}$. A dam separated the domain into two parts. Initially, the water was at rest in the reservoir on the left, with a depth of 0.64 m, while the floodplain on the right was dry. The boundaries of the floodplain were all open, so zero-gradient conditions were specified at all boundaries. A 0.4 m wide section in the middle of the dam was breached instantaneously. Tseng and Chu [11] have demonstrated that no noticeable difference exists between the results for $n = 0$ and $n = 0.02$, where $n$ refers to the Manning's roughness coefficient. This can be attributed to the rapid changes in the flow. In the present simulations, the bed was assumed to be frictionless, and the spatial step was set to 0.04 m. The preset Courant number, $Cr_{\text{Preset}}$, was 0.8, with the minimum and maximum allowed time steps being 0.002 and 0.02 s, respectively. However, it was found that these limitations were never used within the computations. The critical water depth for the wetting/drying, $H_{\min}$, was set to be 0.1 mm, which has been found small enough so that the results are independent of this value.

Figure 3 shows four snapshots of the water surface elevation at four different times. It can be seen that as the bore wave develops downstream, a depression wave travels upstream and is reflected back at the walls, causing the water surface elevation in the reservoir to oscillate at the initial stage. At $t = 0.65\,\text{s}$ the bore wave is about to move out of the computational domain, which is allowed due to the transmissive boundary condition specified around the floodplain. The flow slows down at a later stage, as the water level falls in the reservoir. Figure 4 compares the predicted and measured water depth histories at four locations, with the comparisons



DOI: 10.1002/fld

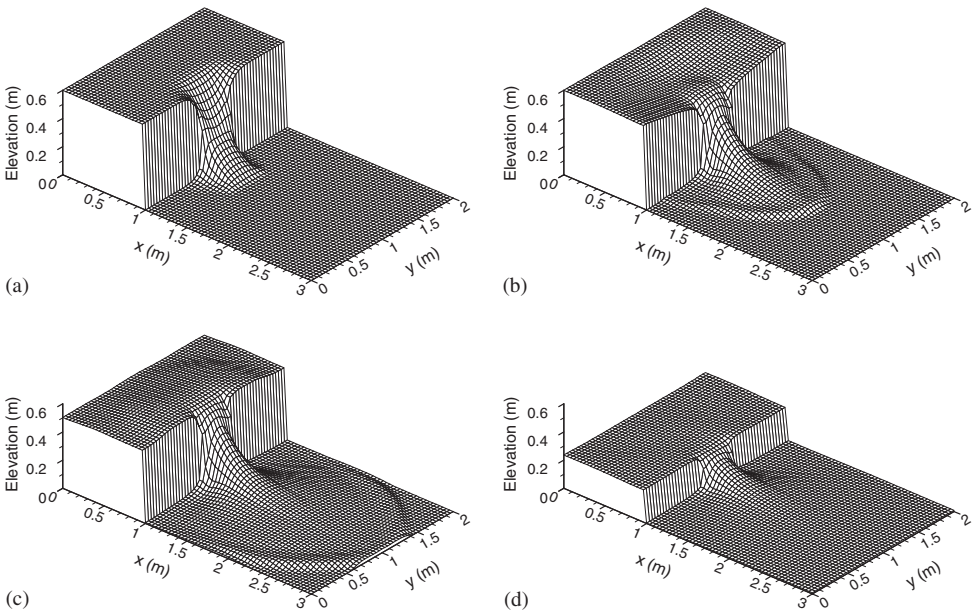


Figure 3. Snapshot of the water surface elevations for a dam-break simulation: (a) $t = 0.1$ s; (b) $t = 0.35$ s; (c) $t = 0.65$ s; and (d) $t = 5$ s.

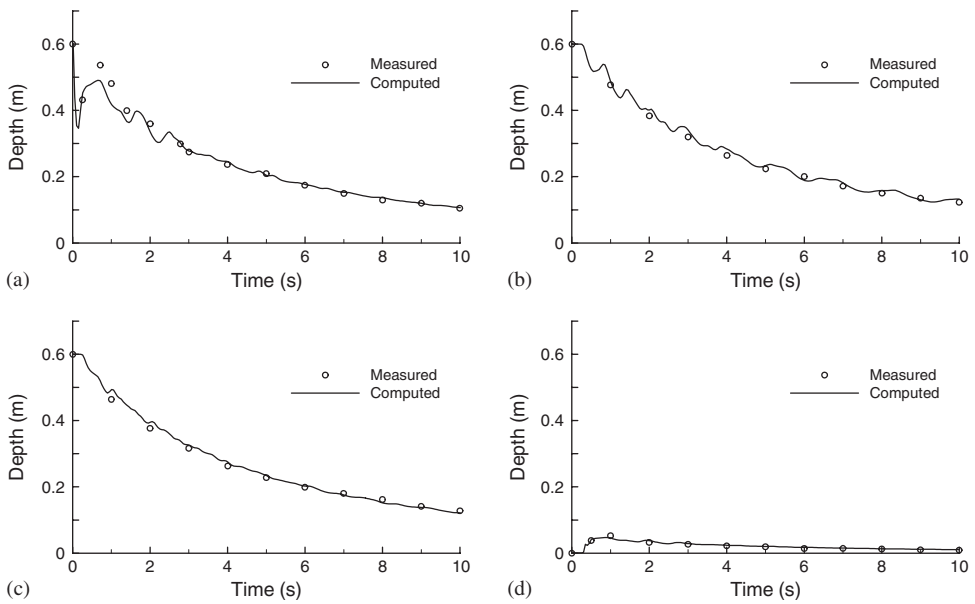


Figure 4. Water depth variations at four locations for a dam-break simulation: (a) ($x = 1$ m, $y = 1$ m); (b) ($x = 0.18$ m, $y = 1$ m); (c) ($x = 0.48$ m, $y = 0.4$ m); and (d) ($x = 1.802$ m, $y = 1.45$ m).



DOI: 10.1002/fld

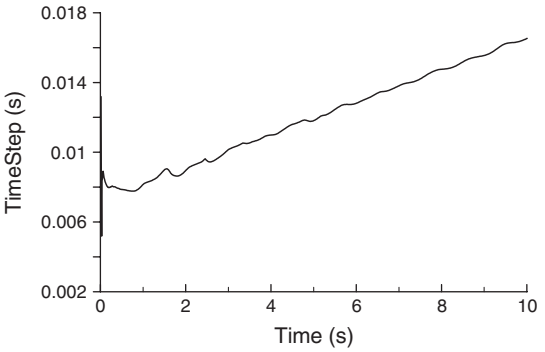


Figure 5. Evolution of the time step for dam-break simulation.

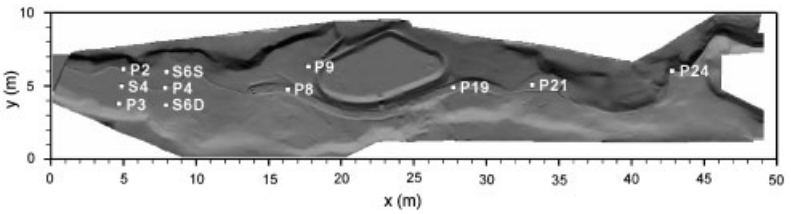


Figure 6. Bed topography of Toce River valley.

being encouraging. A relatively large discrepancy occurs at point ($x = 1$ m, $y = 1$ m), as shown in Figure 4(a). This discrepancy can be attributed to the invalidity of the hydrostatic assumption and the possible experimental inaccuracy at this location, which is also reported in other researches (e.g. References [11, 24]). The overall trend is well captured.

In this computation, the time step was determined by using the adaptive scheme. The evolution of the time step is shown in Figure 5. As time progresses, the time step increases from less than 0.008 s to more than 0.016 s. The uptrend of the curve coincides with the slowing down tendency of the flow.

*Toce river valley flood experiment*

A physical model was built at ENEL (Milano, Italy) under the EU funded project CADAM to study extreme flood events [25]. A 5 km reach of the Toce River valley, located in the northern Italy Alps, was scaled down 100 times to give the dimensions of 55 m × 13 m in the physical model. Figure 6 shows a plan view of the valley model and some gauging positions that will be used in the following verification. Buildings and bridges are not modelled in the present numerical study. However, the ground elevation is raised where the bridge piers are located. Measured flowrate and water level variances were imposed at the inflow tank on the left. Close to the two downstream ends, on the right, there were abrupt drops in the bed elevations, which led to the occurrence of critical flows upstream of the outlets. Therefore, the boundary conditions specified at the outlet should not have any influence on the flow field in the inner domain. To



DOI: 10.1002/fld

simplify the simulations, first-order derivatives of all variables were set to zero at the outlets. There was a reservoir in the middle of the model, which was overtopped in the current configuration. The average slope of the valley was about 2%, with some local slopes far exceeding this value; hence the capability of shock-capturing is essential for any numerical model to simulate this flow well.

The computational domain was composed of 982 $\times$ 205 grids, with a grid size of 0.05 m. The Manning's roughness coefficient was set to 0.0162, as recommended by ENEL. The significant changes in the bed topography and the large inflow rate result in rapid variations in the flow. The wetting/drying process also occurs very quickly along some steep parts of the valley. Due to these conditions, the maximum Courant number, $Cr_{\text{Preset}}$, was set to 0.5 in the computations and the minimum and maximum time steps were 0.002 and 0.02 s, respectively. The whole valley was initially dry, and the minimum water depth, $H_{\min}$, was set to be 5 mm.

Figure 7 shows the hydrographs at some gauging sites along the valley reach. The predicted arrival times of the flood front compare well with the measured values. The agreement in water levels is also generally good. The discrepancies between the ground levels of the corresponding points in the numerical and physical models are due to the fact that they do not coincide exactly with each other. The gauges could be located at any positions in the laboratory model, whereas the numerical predictions had to be taken from discrete grid points. In the present study, the computational domain is overlaid with a uniform, rectangular grid. Due to the ground unevenness, small position errors can result in relatively large disparities in the measured and predicted ground elevations, such as for gauges P2 and P19. Some relatively large discrepancies in the water level at some gauging sites can be attributed to the exclusion of buildings and bridges in the computation. Although these structures do not impose a large influence on the overall water level variations in the numerical modelling, they were found to affect local water depths [25]. Gauges P2, S4 and P3 reside in the same cross-section of the valley, as for the gauges P4, S6S and S6D. It can be seen that the water level is not unique at each cross-section and thus the employment of a 1-D numerical model for this study would be questionable. It is also noticed that at points P3 and S6D the predicted water levels show relatively large errors. P3 is just downstream of some buildings, while S6D is just upstream of some buildings. In the experiments, the buildings in the valley were represented by concrete bricks. Two effects may be caused by these model buildings on the water levels. The water level would have been raised as the result of backwater effects in front of the buildings. At the downstream side of the buildings the water level would have decreased, since the incoming water would have been partly blocked by the buildings. This explains why the predicted water levels at P3 were higher and those at S6D were lower than the measured values.

Figure 8 shows some snapshots of the flood inundation extent along the valley, from which the flooding routes can be seen. The flow cannot be contained in the small channel and the whole valley is wildly inundated. Overtopping of the reservoir is reproduced and small features in the water surfaces can also be seen due to geometrical irregularities and reflections with the valley banks. These observations indirectly confirm the existence of super-critical flows in some regions along the valley.

Figure 9 shows the history of the time step as used in the computation. There was no flow for the first 13 s, and hence a large time step was adopted as expected. The time step became smaller between around 25 and 35 s, after the commencement of simulations, as the flood front reached the wide channel in the upper reaches of the valley and was about to hit the reservoir embankment. Between about 50 and 60 s, the downstream part of the valley began to become



DOI: 10.1002/fld

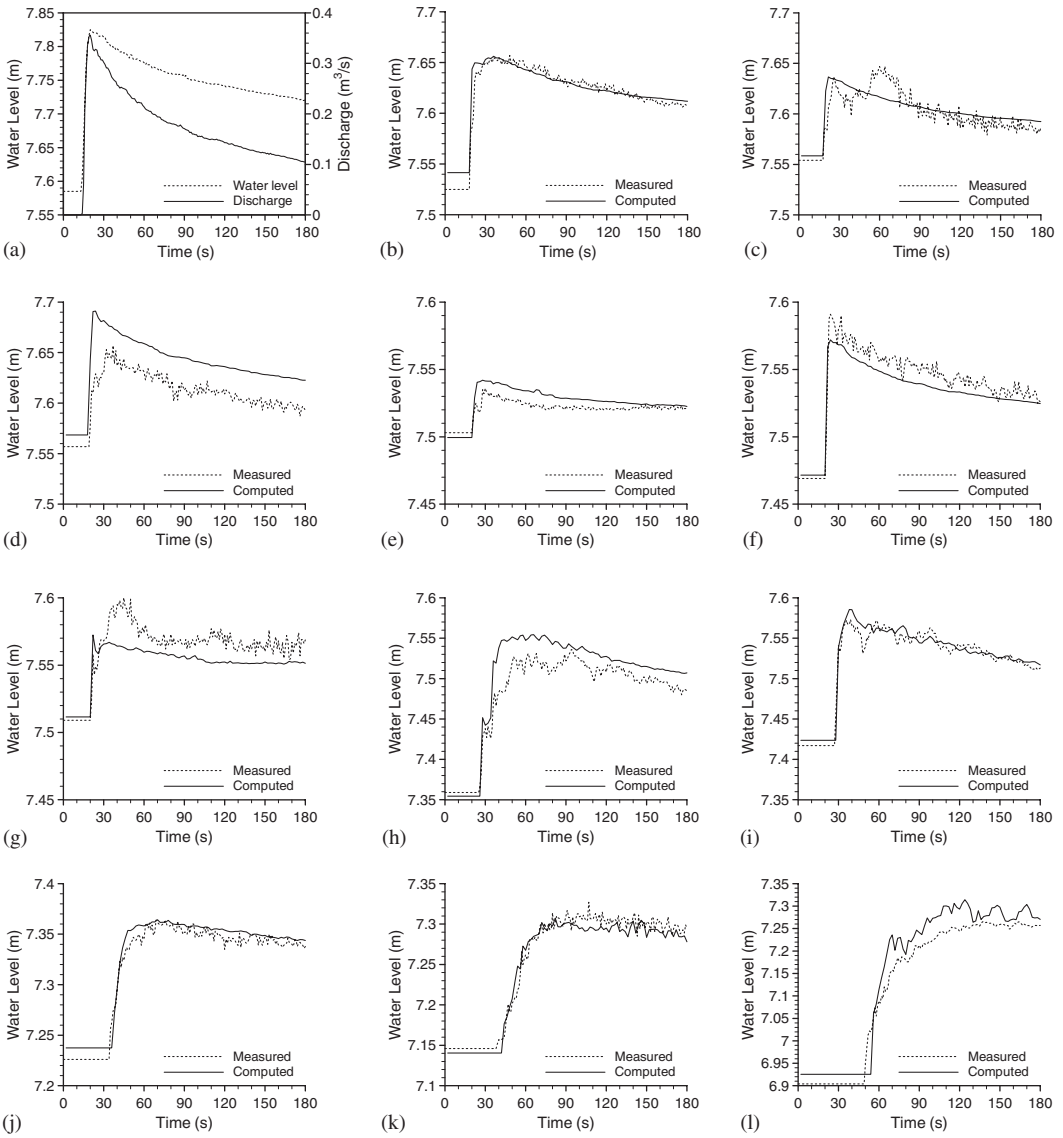


Figure 7. Water level variations at different gauging sites for Toce valley flood: (a) inlet boundary; (b) gauge P2; (c) gauge S4; (d) gauge P3; (e) gauge S6S; (f) gauge P4 (g) gauge S6D; (h) gauge P8; (i) gauge P9; (j) gauge P19; (k) gauge P21; and (l) gauge P24.

inundated, where the bed slope was very steep. As a result, the computational time step was adjusted automatically small. In natural environments drastic variations in the local bed elevations are inevitable. Accordingly, the velocity at the flood wave front may experience drastic changes and will cause the time step to oscillate with time, which is evident in Figure 9.



DOI: 10.1002/fld

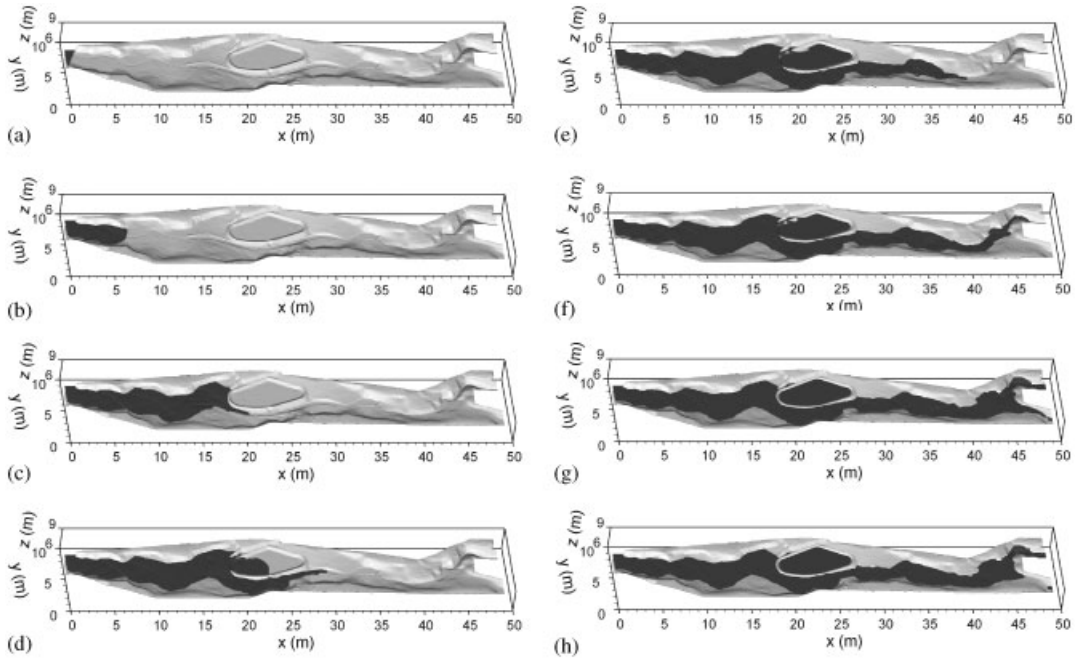


Figure 8. Predicted variance in the flood inundation extent for Toce valley: (a) $t = 10$ s; (b) $t = 20$ s; (c) $t = 30$ s; (d) $t = 40$ s; (e) $t = 50$ s; (f) $t = 60$ s; (g) $t = 120$ s; and (h) $t = 180$ s.

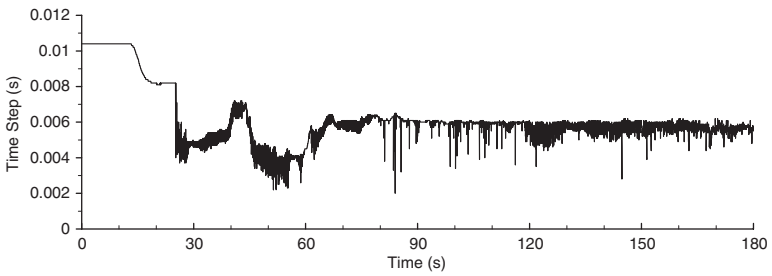


Figure 9. Time step evolution for Toce valley flood simulation.

## SUMMARY AND CONCLUSIONS

A TVD–MacCormack scheme has been applied to solve the SWEs, with second-order accuracy in both time and space. The scheme combines a symmetric TVD scheme with the standard MacCormack scheme. The main advantage of this method is that it is highly efficient. It has been demonstrated in this paper that the same finite difference scheme can be derived from either the conservative or non-conservative form of the SWEs, provided that the source term is discretized in a certain manner. The non-conservative form of the SWEs is employed in the present solution due



DOI: 10.1002/fld

to its simplicity. The bed friction term is included using a partially implicit scheme in regions with small water depths. The wetting/drying representation is incorporated into the operator-splitting and predictor–corrector procedures in the solution. Dry land is recognized at the beginning of each time step, and then zero velocities are assigned with the water elevation being unchanged. Such an approach creates two effects. On the one hand, unrealistic water level gradients are avoided over the dry ground. On the other hand, the solution of finite difference equations is avoided over the dry ground, so the computational speed can be greatly increased if there are a large number of dry cells in the domain. The time step was devised to adjust itself in the computations according to the maximum allowed Courant number. Therefore, large time steps are applied when the flows is slow, likewise smaller time steps are applied when the flow is rapid. By using these techniques, the present numerical model requires only modest computational power, yet has the ability to resolve all flow regimes with a high level of accuracy and stability.

The present model not only simulates the flows in simple configurations well, but also has the capability of handling real flow conditions, such as for a frictional bed, natural topographies and wetting/drying process. Extensive verifications have been made against a large-scale experiment on the Toce River valley flood. The satisfactory agreement between the predicted and measured results show that the numerical methods adopted in the model are reliable and efficient. This model has considerable potential for predicting rapidly varying flows in practical environments.

It should be noted that the predictor and corrector steps of the MacCormack scheme can also be interpreted from the finite volume point of view, where the one-sided flux is taken as the flux between the two grid cells. The TVD term is also written in a strong finite volume form. Therefore, the finite difference and finite volume forms converge into one form for the present model, and the conservation of mass and momentum is strictly satisfied. The present TVD–MacCormack scheme has also been implemented in a general curvilinear coordinate system, so that the irregular boundary can be fitted more accurately.

## ACKNOWLEDGEMENTS

The study is funded by the Engineering and Physical Sciences Research Council as part of the Flood Risk Management Research Consortium programme (Grant GR/S76304).

## REFERENCES

1. Leendertse JJ, Gritton EC. A water quality simulation model for well-mixed estuaries and coastal seas: vol. 2, computation procedures. *Report No. R-708-NYC*, The Rand Corporation, Santa Monica, 1971.
2. Falconer RA. Numerical modelling of tidal circulation in harbours. *Journal of Waterway*, *Port*, *Coastal and Ocean Division* (ASCE) 1980; **106**:31–48.
3. Stelling GS, Wiersma AK, Willemse JBTM. Practical aspects of accurate tidal computations. *Journal of Hydraulic Engineering* (ASCE) 1986; **112**:802–817.
4. Katopodes ND, Strelkoff T. Computing two-dimensional dam-break flood waves. *Journal of Hydraulic Division* (ASCE) 1978; **104**:1269–1287.
5. Chen CL, Armbruster JT. Dam-break wave model: formulation and verification. *Journal of Hydraulic Division* (ASCE) 1980; **106**:747–767.
6. Mools T, Chaudhry MH. Depth-averaged open-channel flow model. *Journal of Hydraulic Engineering* 1995; **121**(6):453–465.
7. Mingham CG, Causon DM. High-resolution finite volume method for shallow water flows. *Journal of Hydraulic Engineering* 1998; **124**(6):605–614.
8. Zoppou C, Roberts S. Catastrophic collapse of water supply reservoirs in urban areas. *Journal of Hydraulic Engineering* (ASCE) 1999; **125**(7):686–695.



DOI: 10.1002/fld

9. Rogers BD, Borthwick AGL, Taylor PH. Mathematical balancing of flux gradient and source terms prior to using Roe's approximate Riemann solver. *Journal of Computational Physics* 2003; **192**:422–451.
10. Wang JS, Ni HG, He YS. Finite-difference TVD scheme for computation of dam-break problems. *Journal of Hydraulic Engineering* (ASCE) 2000; **126**(4):253–262.
11. Tseng MH, Chu CR. Two-dimensional shallow water flows simulation using TVD–MacCormack scheme. *Journal of Hydraulic Research* 2000; **31**:123–131.
12. Vincent S, Caltagirone J-P, Bonneton P. Numerical modelling of bore propagation and run-up on sloping beaches using a MacCormack TVD scheme. *Journal of Hydraulic Research* 2001; **39**(1):41–49.
13. Lin GF, Lai JS, Guo WD. Finite-volume component-wise TVD scheme for 2D shallow water equations. *Advances in Water Resources* 2003; **26**:861–873.
14. Rogers B, Fujihara M, Borthwick AGL. Adaptive Q-tree Godunov-type scheme for shallow water equations. *International Journal for Numerical Methods in Fluids* 2001; **35**:247–280.
15. Liang D, Falconer RA, Lin B. Comparison between TVD–MacCormack and ADI-type solvers of the shallow water equations. *Advances in Water Resources* 2006, http://dx.doi.org/10.1016/j.advwatres.2006.01.005
16. Davis SF. TVD finite difference schemes and artificial viscosity. *ICASE Report No. 84-20*, *NASA CR 172373*, ICASE, NASA Langley Research Center, Hampton, 1984.
17. Louaked M, Hanich L. TVD scheme for the shallow water equations. *Journal of Hydraulic Research* 1998; **36**:(3):363–378.
18. Mingham CG, Causon DM, Ingram DM. A TVD MacCormack scheme for transcritical flow. *Proceedings of the Institution of Civil Engineers*, *Water and Maritime Engineering* 2001; **148**(3):167–175.
19. Garcia-Navarro P, Vazquez-Cendon ME. On numerical treatment of the source terms in the shallow water equations. *Computers and Fluids* 2000; **29**:951–979.
20. Tseng MH. The improved surface gradient method for flows simulation in variable bed topography channel using TVD–MacCormack scheme. *International Journal for Numerical Methods in Fluids* 2003; **43**:71–91.
21. Liang D, Falconer RA, Lin B. Improved numerical modelling of estuarine flows. *Proceedings of the Institution of Civil Engineers*; *Maritime Engineering* 2006; **159**(1):25–35.
22. Liang Q, Borthwick AGL, Stelling G. Simulation of dam- and dyke-break hydrodynamics on dynamically adaptive quadtree grids. *International Journal for Numerical Methods in Fluids* 2004; **46**:127–162.
23. Fraccarollo L, Toro EF. Experimental and numerical assessment of the shallow water model for two-dimensional dam-break type problems. *Journal of Hydraulic Research* 1995; **33**:843–864.
24. Gottardi G, Venutelli M. Central scheme for two-dimensional dam-break flow simulation. *Advances in Water Resources* 2004; **27**:259–268.
25. Testa G. (ed.). *Third CADAM Meeting Proceedings*. Milan: Italy, 1999.



DOI: 10.1002/fld